Title: Quality assurance of hematopoietic stem cells by macrophages determines stem cell clonality

Authors: Samuel J. Wattrus[1,2], Mackenzie L. Smith[1,2], Cecilia Pessoa Rodrigues[1,2], Elliott J. Hagedorn[1,2,†], Bogdan Budnik[3], Leonard I. Zon[1,2*]

Affiliations:

[1] Stem Cell Program and Division of Hematology/Oncology, Boston Children's Hospital and Dana Farber Cancer Institute, Howard Hughes Medical Institute, Harvard Medical School; Boston MA, USA

[2] Harvard Stem Cell Institute, Stem Cell and Regenerative Biology Department, Harvard University; Cambridge, MA

[3] Mass Spectrometry and Proteomics Resource Laboratory, Faculty of Arts and Sciences Division of Science, Harvard University, Cambridge MA, USA

[†] Present address: Section of Hematology and Medical Oncology and Center for Regenerative Medicine, Boston University School of Medicine and Boston Medical Center, Boston, MA, USA

*Corresponding author. Email: zon@enders.tch.harvard.edu

Abstract: Tissue-specific stem cells persist for a lifetime and can differentiate to maintain homeostasis or transform to initiate cancer. Despite their importance, there are no described quality assurance mechanisms for newly formed stem cells. We observed intimate and specific interactions between macrophages and nascent blood stem cells in zebrafish embryos. Macrophage interactions led to two outcomes — removal of cytoplasmic material and stem cell division, or complete engulfment and stem cell death. Stressed stem cells were marked by surface Calreticulin, which stimulated macrophage interactions. Using cellular barcoding, we found that calreticulin knock-down or embryonic macrophage depletion reduced the number of stem cell clones that established adult hematopoiesis. Our work supports a model in which embryonic macrophages determine hematopoietic clonality by monitoring stem cell quality.

Main Text:

Tissue stem cells born during embryogenesis support homeostasis for life. Despite the importance of these cells for proper tissue function, there are no described mechanisms of quality assurance for newly formed stem cells. To explore this possibility, we studied zebrafish embryonic blood development. Hematopoietic stem and progenitor cells (HSPCs) emerge from the ventral wall of the dorsal aorta (VDA), enter circulation, and lodge in the embryonic niche - a vascular plexus called the caudal hematopoietic tissue (CHT) [1, 2]. HSPCs rapidly expand in the CHT for a few days before migrating to the kidney marrow, the adult hematopoietic niche. In the niche, HSPCs interact with a variety of cell types, including vascular endothelial cells, mesenchymal stromal cells, and macrophages [3-6]. *In vivo* clonal labeling studies show that 20 – 30 of the hematopoietic stem cell (HSC) clones born in the VDA ultimately give rise to the adult blood system [7]. It remains unclear if nascent HSCs from the VDA undergo quality assurance before establishing adult hematopoiesis. Here, using live imaging and cellular barcoding, we found discrete interactions between stem cells and embryonic macrophages that regulated the number of long-lived hematopoietic stem cells clones that produce blood in adulthood.

Results:

Macrophages interact with nascent HSPCs in the niche

Macrophages help maintain homeostasis by modulating inflammation, producing cytokines, and patrolling to clear dead, stressed, or aged cells [8-10]. Given these roles in somatic tissue, the enrichment of macrophages in the CHT, and previous observations between macrophages and hematopoietic cells [6], we investigated macrophage function in the niche. We undertook high-resolution live imaging using *mpeg1:mCherry;runx1+23:EGFP* zebrafish

54   embryos with mCherry$^+$ macrophages and EGFP$^+$ HSPCs [4, 11]. Shortly after lodgment in the

55   CHT, HSPCs were physically contacted by a nearby macrophage, their surfaces were scanned,

56   and fluorescent material was taken up by the macrophage (Fig. 1A; Movie S1). From 56 to 106

57   hours post-fertilization (hpf), approximately 20-30% of HSPCs in the niche were engaged by

58   macrophages at any one time (Fig. 1B). These interactions were specific to HSPCs; macrophage

59   engagement with erythrocytes and endothelial cells was significantly lower (0.6 - 3.9% of

60   erythrocytes and 0.5 – 6.7% of endothelial cells) (Fig. S1A). Macrophages physically contacted

61   HSPCs for up to 45 minutes and sometimes extracted fluorescent HSPC material. We classified

62   interactions with fluorescence transfer into two types: "dooming" during which the HSPC was

63   fully engulfed and destroyed by the macrophage, or "grooming" during which the HSPC was left

64   intact and had a small portion of cellular material taken up by the macrophage (Movie S2).

65   Similar interactions were identified in other zebrafish HSPC-reporter lines *cd41:GFP* and

66   *cmyb:GFP* (Figs. S1D-E). To examine if macrophage-HSPC interactions occurred in mammals,

67   we studied E14.5 murine fetal liver sections by immunofluorescence and found that on average

68   33% of c-Kit$^+$ hematopoietic cells were in contact with F4/80$^+$ macrophages. These contacts

69   included c-Kit$^+$ cells being pinched or fully engulfed by macrophages, similar to our

70   observations in zebrafish (Fig. S1F). Overall, these data identify novel macrophage-HSPC

71   interactions in the embryonic hematopoietic niche.

72   To better characterize macrophage-HSPC interactions, we tracked individual HSPCs in

73   the CHT over 4-6 hours and recorded all interactions with macrophages at 2 or 3 days post-

74   fertilization (dpf). We found that 70% of HSPCs eventually experienced prolonged macrophage

75   contact (Fig. 1C). Of these interactions, 13% of HSPCs were groomed, and 13% were fully

76   engulfed and doomed (Fig. 1D). Interestingly, 81% of HSPC divisions occurred within 30

77   minutes following macrophage contact (Fig. 1E). Using the *Tg(EF1a:mAG-zGem(1/100))^{rw0410h}*

78 (Fucci) transgene [12] that labels cells in G2M phase of the cell cycle, we found that

79 approximately 65% of Fucci$^+$ HSPCs contacted macrophages, compared to only 16% of Fucci$^-$

80 HSPCs (Fig. 1F). We next assessed the viability of HSPCs that were engulfed by macrophages.

81 Staining for cell death *in vivo* with Acridine Orange or an Annexin V-YFP construct [13]

82 showed almost no apoptotic HSPCs in the CHT at baseline (Figs. S1B-C). Only after full

83 engulfment by a macrophage did HSPCs exhibit apoptosis (Movie S3). Taken together, these

84 data identify a set of prolonged macrophage-HSPC interactions that either precede HSPC

85 division or death.

86

A subset of primitive macrophages regulates stem cell clone number

88 As we saw proliferation following macrophage-HSPC interactions, we next sought to

89 determine if this might have an effect on the number of stem cell clones that contribute to adult

90 hematopoiesis. We used TWISTR (tissue editing with inducible stem cell tagging via

91 recombination) [14] to combine alteration of embryonic gene expression by morpholino injection

92 with color labeling of HSCs by Zebrabow. *Zebrabow-M;draculin:CreER^{T2}* embryos allow for

93 unique lineage labeling of individual HSC clones at 24 hpf (Fig. 2A) [7, 15]. To deplete

94 embryonic macrophages, we injected the *irf8* morpholino into *Zebrabow-M;draculin:CreER^{T2}*

95 embryos to block macrophage differentiation from the one-cell stage [16] or delivered clodronate

96 liposomes to deplete macrophages at various timepoints: 28 hpf, just prior to HSPC emergence

97 in the VDA, 48 hpf, before HSPC lodgment in the CHT, and 72 hpf, after HSPCs have lodged in

98 the CHT. Analysis of adult marrow myelomonocytes from macrophage-depleted animals

99 revealed a consistent reduction in hematopoietic clonality compared to sibling controls for all

100 timepoints (Fig. 2B). These results demonstrate that embryonic macrophages regulate long-term

101 HSC clone number after VDA emergence.

102   To better understand the mechanism and cellular consequences of macrophage-HSPC

103   interactions observed in the CHT, we pursued transcriptomic analysis of niche macrophages.

104   Because macrophages can take up fluorescent material from HSPCs, we reasoned it would be

105   possible to identify interacting macrophages by their fluorescence profile. Indeed, flow

106   cytometry of dissociated *mpeg1:EGFP;runx1+23:mCherry* embryos revealed a rare population

107   of EGFP$^+$mCherry$^+$ cells (1.67% of all EGFP$^+$ cells), which were morphologically consistent

108   with macrophages containing small HSPC fragments (Fig. 2C). We dissected embryonic

109   zebrafish tails at 72 hpf and purified interacting macrophages (EGFP$^+$mCherry$^+$) and non-

110   interacting macrophages (EGFP$^+$mCherry$^-$) for plate-based single-cell mRNA sequencing. By

111   recording single-cell indices and combining FACS parameters with single-cell transcriptomic

112   profiles, we identified a single population of macrophages which segregated by both gene

113   expression profile and mCherry fluorescence (Fig. 2D). These cells exhibited a relative

114   enrichment for genes associated with engulfment, lysosomal degradation, and cholesterol

115   transporter activity and were marked by genes including *hmox1a, ctsl.1, slc40a1, lrp1ab,* and

116   *c1qa* (Fig. 2D; Fig. S2A) [17]. We validated these data through injection of a fluorescent

117   cholesterol mimic, treatment with Lysotracker dyes, and *in situ* hybridization (Figs. S2B-D).

118   Together, these data show that a transcriptionally distinct and relatively homogenous subset of

119   macrophages engage HSPCs in the CHT for both grooming and dooming behaviors.

120

121   ***Surface Calreticulin drives macrophage-HSPC interactions***

122   To gain insight into the proteinaceous material taken up by macrophages, we pursued

123   few-cell proteomics [18] to compare interacting to non-interacting macrophages isolated from 72

124   hpf embryos. We identified 203 peptides enriched in interacting macrophages potentially

125   representing a repertoire of macrophage proteins involved in the process of macrophage-HSPC

126   interaction or HSPC-derived proteins taken up during the interaction. To identify molecular

127   patterns recognized on HSPCs, we excluded peptides with enriched transcripts in interacting

128   macrophages and compared the remaining peptides to the Cell Surface Protein Atlas [19].

129   Notably, cell surface peptides enriched in EGFP$^+$mCherry$^+$ macrophages included three

130   Calreticulin paralogs: *calr, calr3a,* and *calr3b* (Fig. 3A). Though Calreticulin typically functions

131   as a calcium-binding chaperone protein in the endoplasmic reticulum, it can also be translocated

132   and displayed on the cell surface as an "eat me" signal [9, 10, 20]. Based on our proteomic

133   results, we hypothesized that HSPCs display surface Calreticulin leading to macrophage

134   interaction, and that increasing levels of Calreticulin could lead to grooming and dooming. We

135   found that 30% of *runx1+23$^+$* HSPCs at 72 hpf exhibited classic punctate surface Calr staining

136   [21] (Fig. 3B), similar to the percentage of HSPCs we found interacting with macrophages at this

137   time in the CHT (Fig. 1B). Additionally, the canonical surface Calreticulin binding partners,

138   *lrp1ab* and *c1qa,* were enriched in interacting macrophages by single-cell mRNA-seq (Fig. 2D).

139   Together with complement C1q subcomponent A (*c1qa*), Lrp1ab contacts Calreticulin and forms

140   a bridging complex to initiate phagocytic activity [10, 21, 22]. These results show that

141   Calreticulin decorates the surface of a subset of HSPCs and may signal for macrophage

142   interaction.

143   To study the role of Calreticulin in macrophage-HSPC interactions, we used morpholinos

144   to knock-down gene expression and quantified these interactions. We observed a significant

145   reduction in the percentage of HSPCs engaged by macrophages after either *calr3a* or *calr3b*

146   knock-down (Fig. 3C). This effect was reversed in genetic rescue experiments (Figs. S3A-B).

147   We generated parabiotic fusions to join circulation of embryos with or without calreticulin

148   knock-down and found that HSPCs with *calr3a* knock-down had reduced interactions with

149   unperturbed macrophages, indicating that Calreticulin presentation is likely HSPC autonomous

150 (Fig. S3C). We then tested the effect of a constitutively surface-translocated form of Calreticulin

151 expressed under the HSPC specific *runx1+23* enhancer [4] (Fig. 3D). The mosaic nature of the

152 expression of this construct allows simultaneous comparison of HSPCs with or without

153 Calreticulin overexpression in the same embryo. HSPCs overexpressing either *calr, calr3a,* or

154 *calr3b* were 3 to 5-fold more likely to interact with macrophages compared to unperturbed

155 HSPCs in the same embryos (Fig. 3E). When *calr3a* or *calr3b* were knocked down, we found

156 that the frequency of both grooming and dooming type interactions dropped, with a more severe

157 decrease in dooming (Fig. S3D). Conversely, when levels of Calreticulin were elevated with

158 overexpression constructs, nearly all expressing cells were doomed (Fig. S3E). Taken together,

159 these data show that surface display of Calreticulin promotes macrophage-HSPC interactions in

160 the CHT and suggest that differing levels of Calreticulin determine if an HSPC is groomed or

161 doomed.

162   To determine if Calreticulin-dependent interactions during development were responsible

163 for regulating HSC clone number into adulthood, we knocked down *calr3a* or *calr3b* during

164 development and color labeled HSCs at 24 hpf. At 2 months, adult marrow analysis in these

165 animals showed a significant reduction in the number of HSC clones compared to sibling

166 controls (Fig. 3F). These data show that Calreticulin-dependent interactions in development

167 support a greater number of long-lived HSC clones.

168

169 ***Macrophages buffer HSPC stress and promote cell cycling***

170   We next wanted to assess calreticulin function in HSPC development. To analyze

171 changes to HSPC budding in the VDA we injected either the *irf8, calr3a,* or *calr3b* morpholino

172 into *cd41:GFP;kdrl:mCherry* embryos, which permit visualization of the endothelial-to-

173 hematopoietic transition [23]. Quantification of GFP$^+$mCherry$^+$ cells in the aortic floor from 32 –

174 46 hpf revealed no significant difference in HSPC budding with loss of macrophages or

175 calreticulin (Fig. S4A). Serial imaging and quantification of *cd41:GFP⁺* cells in the CHT over

176 early development revealed that knock-down of *calr3a* or *calr3b* did not affect HSPC numbers

177 through 60 hpf, but later reduced HSPCs at 72 and 84 hpf (Figs. S4B-C). The loss of HSPCs in

178 *irf8, calr3a,* and *calr3b* morphants was not due to apoptosis (Fig. S4D). Rather, depletion of

179 macrophages or knock-down of *calr3a* or *calr3b* significantly reduced the fraction of

180 proliferative HSPCs in the CHT at 72 hpf, as measured by EdU incorporation (Fig. 4A). This is

181 in agreement with the association of macrophage-HSPC interactions with cell division identified

182 by live imaging of the CHT (Figs. 1E-F). These data show that Calreticulin-dependent

183 macrophage-HSPC interactions serve to expand and maintain HSPCs during early development

184 by promoting proliferation in the CHT.

185   To molecularly evaluate the effect of macrophage interactions on HSPCs and the

186 qualities of HSPCs that lead to surface Calreticulin, we injected *runx1+23:mCherry* embryos

187 with the *irf8* or control morpholino and performed single-cell mRNA-seq on sorted HSPCs at 72

188 hpf. This analysis identified a subset of HSPCs enriched in *irf8* morphants marked by genes

189 associated with FoxO activity and cellular senescence (Figs. 4B-C). FoxO activity is induced in

190 response to elevated reactive oxygen species (ROS) and mediates detoxification of ROS and

191 repair of ROS-induced damage [24, 25]. The enrichment of HSPCs with FoxO activity in *irf8*

192 morphants suggested that there may be ROS accumulation in stem cells during embryogenesis

193 which is ordinarily resolved by macrophages. In murine HSCs, FoxO deletion results in

194 dysregulation of apoptosis, cell cycling, and colony formation due to resulting ROS

195 accumulation [26]. In agreement with this, flow cytometric analysis identified higher levels of

196 ROS in *runx1+23⁺* HSPCs marked by surface Calreticulin, with significant correlation between

197 levels of ROS and surface Calreticulin (Spearman's Correlation; ****P< 2.2e-16) (Fig. 4D).

8

198   Treatment with the ROS inhibitor diphenylene iodonium reduced macrophage-HSPC

199   interactions at 3 dpf (Fig. 4E). These results show that in the absence of macrophages, a

200   population of HSPCs with elevated ROS accumulates, and this is associated with surface

201   Calreticulin and subsequent macrophage interactions.

202   Embryos injected with the *irf8* morpholino also lost a subset of HSPCs marked by genes

203   associated with cell cycling and ERK/MAPK signaling (Figs. 4B-C). In accordance with this,

204   depleting macrophages or inhibiting ERK/MAPK activity from 48-72 hpf reduced HSPC

205   proliferation without perturbing the frequency of macrophage-HSPC interactions. ERK/MAPK

206   inhibition in the context of macrophage depletion did not further reduce proliferation, indicating

207   that macrophages likely stimulate division via this pathway (Fig. S5A). As inflammation is a

208   critical determinant of HSPC proliferation in development [27, 28], we reasoned that pro-

209   proliferative cytokines produced by the macrophages, such as *il1b* and *tnfb*, could be responsible

210   for the cell cycling phenotype (Fig. S5B) [28, 29]. To demonstrate this, we rescued HSPC

211   proliferation after macrophage depletion by heat shock overexpression of *il1b* [28] (Fig. 4F).

212   These results show that HSPC cycling in the CHT is mediated partly through ERK/MAPK and

213   that signals produced by CHT macrophages including *il1b* can induce HSPC proliferation.

214

215   **Discussion:**

216   Our data support a model in which macrophages of the embryonic niche vet the quality of

217   newly formed HSPCs through prolonged physical contact leading to either expansion or

218   engulfment. This process is mediated by the display of Calreticulin on the cell surface, which is

219   associated with elevated ROS. It has previously been reported that metabolic shifts during HSPC

220   generation in the VDA elevate ROS to mediate HIF1α stabilization [30]. Cells with high levels

221   of ROS are also at elevated risk for DNA damage and dysfunction [24, 25]. Our work suggests

that while ROS generation in the VDA promotes stem cell emergence, titration of ROS levels is ultimately required for normal hematopoiesis. Although we see no evidence for *vcam1* expression in embryonic macrophages, previous imaging studies have indicated a role for macrophages in HSPC homing [6]. Macrophages are involved in HSPC mobilization in the zebrafish aorta [31], and murine macrophage subpopulations facilitate HSPC engraftment [32]. In contrast, our studies find that macrophages in the CHT remove stem cell clones with high surface Calreticulin which have not downregulated ROS production. Healthy HSPCs with low-to-moderate levels of ROS and Calreticulin experience prolonged macrophage contact, avoid complete engulfment, and receive pro-proliferative signals to enable competition for marrow colonization.

Our work establishes that stem cells are quality assured during development, and this impacts the clones that contribute to blood formation in adulthood. Calreticulin functions as an "eat me" molecule that initiates macrophage-HSPC interaction and leads to programmed cell clearance or stem cell expansion. Orthologs of CD47 and SIRPα, "don't eat me" signals, have not been identified in zebrafish, but other primitive signals could participate in macrophage behaviors. This quality assurance mechanism may also be utilized in adulthood in response to environmental stress, such as during marrow transplantation or in clonal stem cell disorders including myelodysplasia and leukemia. Macrophages may selectively expand or remove clones of tissue-specific stem cells in other systems similar to our findings. Other tissue stem cells rely on macrophages to assure adequate tissue regeneration [33], and this could occur through selective proliferation of certain clones. Manipulating this quality assurance mechanism may have significant therapeutic implications for disorders of stem cell biology and tissue regeneration.

References:

1. Kissa, K. and P. Herbomel, *Blood stem cells emerge from aortic endothelium by a novel type of cell transition.* Nature, 2010. **464**(7285): p. 112-5.

2. Bertrand, J.Y., et al., *Haematopoietic stem cells derive directly from aortic endothelium during development.* Nature, 2010. **464**(7285): p. 108-11.

3. Murayama, E., et al., *Tracing hematopoietic precursor migration to successive hematopoietic organs during zebrafish development.* Immunity, 2006. **25**(6): p. 963-75.

4. Tamplin, O.J., et al., *Hematopoietic stem cell arrival triggers dynamic remodeling of the perivascular niche.* Cell, 2015. **160**(1-2): p. 241-52.

5. Hagedorn, E.J., et al., *Transcription factor induction of vascular blood stem cell niches in vivo.* bioRxiv, 2021: p. 2021.11.03.467105.

6. Li, D., et al., *VCAM-1(+) macrophages guide the homing of HSPCs to a vascular niche.* Nature, 2018. **564**(7734): p. 119-124.

7. Henninger, J., et al., *Clonal fate mapping quantifies the number of haematopoietic stem cells that arise during development.* Nat Cell Biol, 2017. **19**(1): p. 17-27.

8. Herbomel, P., B. Thisse, and C. Thisse, *Ontogeny and behaviour of early macrophages in the zebrafish embryo.* Development, 1999. **126**(17): p. 3735-45.

9. Feng, M., et al., *Macrophages eat cancer cells using their own calreticulin as a guide: roles of TLR and Btk.* Proc Natl Acad Sci U S A, 2015. **112**(7): p. 2145-50.

10. Feng, M., et al., *Programmed cell removal by calreticulin in tissue homeostasis and cancer.* Nat Commun, 2018. **9**(1): p. 3194.

11. Ellett, F., et al., *mpeg1 promoter transgenes direct macrophage-lineage expression in zebrafish.* Blood, 2011. **117**(4): p. e49-56.

12. Sugiyama, M., et al., *Illuminating cell-cycle progression in the developing zebrafish embryo.* Proc Natl Acad Sci U S A, 2009. **106**(49): p. 20812-7.

13. van Ham, T.J., et al., *Live imaging of apoptotic cells in zebrafish.* FASEB J, 2010. **24**(11): p. 4336-42.

14. Avagyan, S., et al., *Resistance to inflammation underlies enhanced fitness in clonal hematopoiesis.* Science, 2021. **374**(6568): p. 768-772.

15. Pan, Y.A., et al., *Zebrabow: multispectral cell labeling for cell tracing and lineage analysis in zebrafish.* Development, 2013. **140**(13): p. 2835-46.

16. Shiau, C.E., et al., *Differential requirement for irf8 in formation of embryonic and adult macrophages in zebrafish.* PLoS One, 2015. **10**(1): p. e0117513.

17. Zhou, Y., et al., *Metascape provides a biologist-oriented resource for the analysis of systems-level datasets.* Nat Commun, 2019. **10**(1): p. 1523.

18. Budnik, B., et al., *SCoPE-MS: mass spectrometry of single mammalian cells quantifies proteome heterogeneity during cell differentiation.* Genome Biol, 2018. **19**(1): p. 161.

19. Bausch-Fluck, D., et al., *A mass spectrometric-derived cell surface protein atlas.* PLoS One, 2015. **10**(3): p. e0121314.

20. Chao, M.P., et al., *Calreticulin is the dominant pro-phagocytic signal on multiple human cancers and is counterbalanced by CD47.* Sci Transl Med, 2010. **2**(63): p. 63ra94.

21. Gardai, S.J., et al., *Cell-surface calreticulin initiates clearance of viable or apoptotic cells through trans-activation of LRP on the phagocyte.* Cell, 2005. **123**(2): p. 321-34.

22. Ogden, C.A., et al., *C1q and mannose binding lectin engagement of cell surface calreticulin and CD91 initiates macropinocytosis and uptake of apoptotic cells.* J Exp Med, 2001. **194**(6): p. 781-95.

23. Kissa, K., et al., *Live imaging of emerging hematopoietic stem cells and early thymus colonization.* Blood, 2008. **111**(3): p. 1147-56.

24. Kops, G.J., et al., *Forkhead transcription factor FOXO3a protects quiescent cells from oxidative stress.* Nature, 2002. **419**(6904): p. 316-21.

25. Tran, H., et al., *DNA repair pathway stimulated by the forkhead transcription factor FOXO3a through the Gadd45 protein.* Science, 2002. **296**(5567): p. 530-4.

26. Tothova, Z., et al., *FoxOs are critical mediators of hematopoietic stem cell resistance to physiologic oxidative stress.* Cell, 2007. **128**(2): p. 325-39.

27. Espin-Palazon, R., et al., *Proinflammatory signaling regulates hematopoietic stem cell emergence.* Cell, 2014. **159**(5): p. 1070-1085.

28. Frame, J.M., et al., *Metabolic Regulation of Inflammasome Activity Controls Embryonic Hematopoietic Stem and Progenitor Cell Production.* Dev Cell, 2020. **55**(2): p. 133-149 e6.

29. Pietras, E.M., et al., *Chronic interleukin-1 exposure drives haematopoietic stem cells towards precocious myeloid differentiation at the expense of self-renewal.* Nat Cell Biol, 2016. **18**(6): p. 607-18.

30. Harris, J.M., et al., *Glucose metabolism impacts the spatiotemporal onset and magnitude of HSC induction in vivo.* Blood, 2013. **121**(13): p. 2483-93.

31. Travnickova, J., et al., *Primitive macrophages control HSPC mobilization and definitive haematopoiesis.* Nat Commun, 2015. **6**: p. 6227.

32. Chow, A., et al., *Bone marrow CD169+ macrophages promote the retention of hematopoietic stem and progenitor cells in the mesenchymal stem cell niche.* J Exp Med, 2011. **208**(2): p. 261-71.

33. Ratnayake, D., et al., *Macrophages provide a transient muscle stem cell niche via NAMPT secretion.* Nature, 2021. **591**(7849): p. 281-287.

34. Lin, H.F., et al., *Analysis of thrombocyte development in CD41-GFP transgenic zebrafish.* Blood, 2005. **106**(12): p. 3803-10.

35. North, T.E., et al., *Prostaglandin E2 regulates vertebrate haematopoietic stem cell homeostasis.* Nature, 2007. **447**(7147): p. 1007-11.

36. Chi, N.C., et al., *Foxn4 directly regulates tbx2b expression and atrioventricular canal formation.* Genes Dev, 2008. **22**(6): p. 734-9.

37. Mosimann, C., et al., *Chamber identity programs drive early functional partitioning of the heart.* Nat Commun, 2015. **6**: p. 8146.

38. Ganis, J.J., et al., *Zebrafish globin switching occurs in two developmental stages and is controlled by the LCR.* Dev Biol, 2012. **366**(2): p. 185-94.

39. Muraro, M.J., et al., *A Single-Cell Transcriptome Atlas of the Human Pancreas.* Cell Syst, 2016. **3**(4): p. 385-394 e3.

40. van den Brink, S.C., et al., *Single-cell sequencing reveals dissociation-induced gene expression in tissue subpopulations.* Nat Methods, 2017. **14**(10): p. 935-936.

41. Hashimshony, T., et al., *CEL-Seq2: sensitive highly-multiplexed single-cell RNA-Seq.* Genome Biol, 2016. **17**: p. 77.

42. Li, H. and R. Durbin, *Fast and accurate short read alignment with Burrows-Wheeler transform.* Bioinformatics, 2009. **25**(14): p. 1754-60.

43. Grun, D., L. Kester, and A. van Oudenaarden, *Validation of noise models for single-cell transcriptomics.* Nat Methods, 2014. **11**(6): p. 637-40.

44. Stuart, T., et al., *Comprehensive Integration of Single-Cell Data.* Cell, 2019. **177**(7): p. 1888-1902 e21.

339 45.   Herman, J.S., Sagar, and D. Grun, *FateID infers cell fate bias in multipotent progenitors*
340   *from single-cell RNA-seq data.* Nat Methods, 2018. **15**(5): p. 379-386.
341 46.   Grun, D., *Revealing dynamics of gene expression variability in cell state space.* Nat
342   Methods, 2020. **17**(1): p. 45-49.
343 47.   Thisse, C. and B. Thisse, *High-resolution in situ hybridization to whole-mount zebrafish*
344   *embryos.* Nat Protoc, 2008. **3**(1): p. 59-69.
345 48.   Mosimann, C. and L.I. Zon, *Advanced zebrafish transgenesis with Tol2 and application*
346   *for Cre/lox recombination experiments.* Methods Cell Biol, 2011. **104**: p. 173-94.
347 49.   Tang, J.C., et al., *Detection and manipulation of live antigen-expressing cells using*
348   *conditionally stable nanobodies.* Elife, 2016. **5**.
349 50.   Specht, H., et al., *Automated sample preparation for high-throughput single-cell*
350   *proteomics.* bioRxiv, 2018: p. 399774.
351 51.   Kall, L., J.D. Storey, and W.S. Noble, *Non-parametric estimation of posterior error*
352   *probabilities associated with peptides identified by tandem mass spectrometry.*
353   Bioinformatics, 2008. **24**(16): p. i42-8.
354 52.   Hagedorn, E.J., et al., *Generation of Parabiotic Zebrafish Embryos by Surgical Fusion of*
355   *Developing Blastulae.* J Vis Exp, 2016(112).
356

Materials and Methods

Animal models

Wild-type zebrafish AB, *casper* or *casper*-EKK, and transgenic lines *cd41:GFP* [34],

runx1+23:EGFP [4], *runx1+23:mCherry* [*runx1+23:NLS-mCherry*] [4], c*myb:GFP* [35]*,*

kdrl:mCherry [*kdrl:Hsa.hras-mCherry*] [36], *Zebrabow-M* [15] *draculin:CreER^{T2}*[37],

mpeg1:EGFP [11], *mpeg1:mCherry* [11]*, mpeg1:BFP* [*mpeg1:TagBFP*]*, LCR:EGFP* [38],

EF1a:mAG-zGem(1/100))^{rw0410h} [12], and *hsp70l:il1b* [28] were used in this study. Alternative

gene names are listed in parenthesis and full transgene names are listed in brackets. Wildtype

C57BL/6J mice (Jackson Labs stock #000664) were also used in this study. All animals were

housed at Boston Children's Hospital and handled according to approved Institutional Animal

Care and Use Committee (IACUC) of Boston Children's Hospital protocols.

Single-cell mRNA-seq preparation

For single-cell mRNA-sequencing of embryonic macrophages, several hundred 72 hpf

runx1+23:mCherry;mpeg1:EGFP embryos were anesthetized with tricaine overdosed and

13

372   transected with a scalpel to harvest tail tissue. For analysis of HSPCs from *irf8* morpholino

373   injected animals, 72 hpf *runx1+23:mCherry* embryos were anesthetized with tricaine and

374   chopped with razor blades. Tissue was dissociated using Liberase (Roche) and cells were

375   harvested by FACS using a BD FACSAria II (BD Biosciences). We used 3nM DRAQ7 (Abcam)

376   for Live/Dead staining. Viable single cells were FACS sorted into 384-well plates, called cell

377   capture plates, that were ordered from Single Cell Discoveries, a single-cell sequencing service

378   provider based in the Netherlands. Each well of a cell capture plate contains a small 50 nl droplet

379   of barcoded primers and 10 µl of mineral oil (Sigma M8410). After sorting, plates were

380   immediately spun and placed on dry ice. Plates were stored at -80° C.

381   Plates were shipped on dry ice to Single Cell Discoveries, where single-cell mRNA

382   sequencing was performed according to an adapted version of the SORT-seq protocol [39] with

383   primers described in [40]. Cells were heat-lysed at 65° C followed by cDNA synthesis After

384   second-strand cDNA synthesis, all the barcoded material from one plate was pooled into one

385   library and amplified using in vitro transcription. Following amplification, library preparation

386   was done following the CEL-Seq2 protocol [41] to prepare a cDNA library for sequencing

387   using TruSeq small RNA primers (Illumina). The DNA library was paired-end sequenced on an

388   Illumina Nextseq™ 500, high output, with a 1×75 bp Illumina kit (read 1: 26 cycles, index read:

389   6 cycles, read 2: 60 cycles)

390

391   Single-cell mRNA-seq analysis

392   For each dataset, paired-end reads were aligned to the zebrafish transcriptome using BWA [42].

393   Data was demultiplexed as described in [43]. Mapping and generation of count tables were

394   automated using the MapAndGo script. We corrected read counts for UMI barcodes by removing

395   duplicate reads that had identical library, cellular, and molecular barcodes and mapped to the

396   same gene. Transcript counts were adjusted using Poissonian counting statistics to yield the

397   number of UMIs detected per cell. Counts were imported into R using the Seurat suite version

398   3.0 [44]. Low quality cells were filtered out by keeping only cellular barcodes with greater than

399   500 UMIs per cell, greater than 500 genes per cell, and less than 9 percent of reads mapping to

400   mitochondrial genes. Data were log normalized and scaled, and the 2000 most variable genes

401   were identified. We reduced dimensionality using PCA, selecting 15 PCs that explained the

402   majority of variation in the data. PC loadings were used as input for a graph-based approach to

403   cluster cells by type and as input for Uniform Manifold Approximation and Projection (UMAP).

404   Differentially expressed genes were identified using a Wilcox Rank Sum test to compare count

405   data between clusters. Significant genes were obtained using an FDR threshold of 0.05. To

406   combine single cell transcriptional profiles with FACS profiles, individually sorted cell indices

407   were merged with single cell RNA data by matching well ID.

408   For further analysis of purified *runx1+23:mCherry⁺* cells, we discarded the reads

409   mapping to ERCC spike-ins and cells having transcripts correlating to mitochondrial and

410   ribosomal genes with a Pearson's correlation coefficient > 0.65. Next, RaceID3 analysis [45] was

411   initiated with mintotal =3000, minexp =5, minnumber=5, and internal batch effect using the

412   plates ID as input. For the outlier identification we used probthr =0.001 and outlog=2. Then, the

413   transcription distance was calculated using the compdist() function, followed by clustexp() using

414   the following parameters: clustnr= 30, bootnr =50, samp=1000, metric = pearsonto, sat= TRUE,

415   FUNcluster = "hclust" to identified the initial number of clusters present in our dataset. We used

416   the plotjaccard() function to identify the saturation point and re-calculated the clustexp() function

417   using cln=8 and sat=FALSE. After RaceID3 benchmarking, we performed VarID analysis [46]

418   to infer the local neighborhoods of cells in the same. To determine the k-nearest neighbors for

419   each cell in gene expression space, and test if the links are supported by a negative binomial joint

420   distribution of gene expression we applied the pruneKnn function with the following parameters:

421   d= gene expression values from RaceID3 dataset, pcaComp=100, regNB=TRUE, batch=plate ID

422   name, knn=10, alpha =1, ngenes=2000 and links with probabilities lower than pvalue < 0.01

423   were removed. To visualize the VarID analysis, we performed Louvain clustering and UMAPs

424   reduction for cluster visualization were generated using compumap() function. To increase our

425   HSPC cluster resolution we removed the erythrocytes and myeloid cells clusters from our single-

426   cell object using the reduceset() function. Differentially expressed genes were identified by the

427   differential gene expression function diffexpnb() from the RaceID3 (v0.1.4) algorithm with

428   multiple testing corrected by the Benjamini-Hochberg method set significance as $p<0.01$.

429   ClurterProfiler software version 4.0 (https://doi.org/10.1016/j.xinn.2021.100141) was run to

430   evaluate the biological pathways associated with each of differentially expressed genes (DEG)

431   from the VarID identified clusters. The parameters applied were: all identified transcript set as

432   universe, the DEG form each target cluster set as gene target list and enrichment strategy set

433   either as enrichGO() or enrichKEGG(). Significance was scored by adjusted Benjamin-Hochberg

434   with p-value = 0.01 and qvalue = 0.05.

435

436   <u>Whole mount in situ hybridization (WISH)</u>

437   *In situ* hybridization was performed using a standard protocol [47]. *In situ* probes were generated

438   by PCR amplification using a cDNA or plasmid template followed by reverse transcription with

439   digoxigenin-linked nucleotides. Primer sequences for all WISH probes used in this paper are

440   provided in Supplementary Table 1.

441

442   <u>Transgenesis</u>

443   Transgenic lines were established as previously described [48]. The *mpeg1:TagBFP* line was

444   generated by PCR amplification of the pCAG-dGBP1-TagBFP plasmid, D-TOPO cloning into

445   pME Gateway, and LR Gateway Reaction to generate constructs with the *mpeg1* promoter

446   driving *TagBFP,* followed by an SV40 polyA signal sequence, all flanked by Tol2 integration

447   sites. The pCAG-dGBP1-TagBFP plasmid was a gift from Connie Cepko [49] (Addgene plasmid

448   #80086). Calreticulin overexpression constructs were generated by PCR amplification off of

449   genomic DNA, followed by D-TOPO cloning and LR gateway reactions as noted before. The

450   fidelity of all constructs was confirmed by sequencing prior to injection.

451

452   Microscopy and image analysis

453   Time-lapse microscopy was performed using a Yokogawa CSU-X1 spinning disk mounted on an

454   inverted Nikon Eclipse Ti microscope equipped with dual Andor iXon EMCCD cameras and a

455   climate controlled (maintained at 28.5˚C) motorized x-y stage to facilitate tiling and imaging of

456   multiple specimens simultaneously. Screening of injected constructs and imaging of WISH

457   embryos was performed using a Nikon SMZ18 stereomicroscope equipped with a Nikon DS-Ri2

458   camera. All images were acquired using NIS-Elements (Nikon), blinded, and processed using

459   Imaris (Bitplane). Specimens were mounted in 0.8% LMP agarose with tricaine (0.16 mg/ml) in

460   glass bottom 6-well plates and covered with E3 media containing tricaine (0.16 mg/ml).

461

462   Flow cytometry

463   To collect kidney marrows, adult zebrafish (2 to 9-months-old) were anaesthetized with 0.02%

464   tricaine in fish water and dissected under a Leica MZ75 light microscope. The soft tissue of the

465   kidney marrow was placed in cold 0.9x DPBS (Gibco) with 2% fetal bovine serum (FBS,

466   Gemini Bio-Products) and 1 USP units/mL heparin (Sigma), and then mechanically dissociated

17

467   by repeated pipetting into single cell suspension, and passed through a 40-μm nylon mesh 5-10

468   minutes prior to analysis. To collect embryonic samples, embryos were chopped with a razor

469   blade in cold PBS and then incubated in Liberase (Roche) for 20 minutes at 37˚C before filtering

470   the dissociated cells through a 40 μm filter and transferring to 2% FBS. For samples stained for

471   Calreticulin, Liberase was not added. Cells were blocked in 5% Normal Goat Serum + 0.5%

472   Sodium Azide in cold PBS for 20 minutes, washed, and incubated with a Chicken anti-

473   Calreticulin antibody (abcam ab94935, 1:1000) for 30 minutes on ice. Samples were then

474   washed and incubated with a Goat anti-Chicken Alexa Fluor 488 antibody (Invitrogen A11039,

475   1:1000) for 25 minutes at room temperature, protected from light. CellROX Deep Red

476   (Invitrogen C10422) and AnnexinV-FITC (BD Biosciences) staining was performed according

477   to manufacturer instructions. We used 3nM DRAQ-7 for live/dead stain (Abcam). Flow

478   cytometric analysis was performed on a BD FACSAria II with special order 445nm laser for

479   CFP detection when using Zebrabow (BD Biosciences). Gates were drawn using negative and

480   isotype matching controls. Data were analyzed with FlowJo software version 10.

481

482   Zebrabow color labelling

483   At 24 hours post fertilization (hpf) embryos were transferred to 6-well plates at a density of 25-

484   35 embryos per well and treated with 15 μM 4-hydroxytamoxifen (4-OHT) for 3-5 hours in the

485   dark at 28.5°C.

486

487   Zebrabow analysis

488   Color barcodes from Zebrabow kidney marrow samples were quantified using previously

489   published pipelines [7] adapted to a Python-based interface. The granulocytic color output was

490   chosen as a read out of clonal changes as these cells have a short half-life and reflect changes in

18

491   the HSPC clonal output in a timely manner. Only zebrafish with greater than 75% recombination

492   efficiency were processed. All samples were blinded prior to analysis.

493

494   Drug treatment

495   Drugs were added to embryo E3 media. MEK1/2 inhibition was done using PD98059 (Sigma) at

496   48 hpf at a concentration of 15 µM. Diphenylene iodonium (Sigma) was added to embryos at 48

497   hpf at a concentration of 100 µM.

498

499   Morpholino injections

500   Morpholinos (GeneTools) were resuspended to 300 µM in nuclease free water, heated to 65°C

501   for 5 minutes, and kept at room temperature. Embryos were injected with 1 nanoliter into the

502   yolk at the 1-4 cell stage with either 3 ng (*calr, calr3a, calr3b, std*) or 5 ng (*irf8, std*) of

503   morpholino. Morpholino sequences are listed in Supplemental Table 2.

504

505   Liposome injection

506   Zebrafish embryos were dechorionated and anesthetized with tricaine (0.16mg/ml) on flat

507   agarose disks. Approximately 1.5 nanoliters of liposomes loaded with either clodronate or PBS

508   (Liposoma) were injected directly into circulation into either the caudal vein (28 hpf) or the duct

509   of Cuvier (48 hpf, 72 hpf).

510

511   Few-cell proteomics

512   Cell pellets were submitted after FACS sort for mass spec analysis. Cell pellets were

513   resolubilized in pure water and undergoing mPOP procedure [50], briefly, frozen cells in water

514 straight from -80C freezer were put into heated 96 well plate shaker at 95 C for 5 min. After cells

515 were chilled to room temperature trypsin was added for 3 hours digest procedure at 38 C.

516 Digested proteins were labeled with TMT11plex (Tandem Mass Tags) labels (Thermo-Fisher,

517 Germany) according to the previously published procedure SCOPE-MS [18]. After labeling

518 procedure all samples were quenched with 5% hydroxyl solution and pulled together as one

519 sample for further mass spectrometry analysis. Two consecutive LC-MS/MS experiments were

520 performed on HFX Orbitrap (Thermo-Fisher, CA) equipped with UltiMate 3000 HPLC Nano

521 tandem pump (Thermo-Fisher, CA). Peptides were separated onto PharmaFluidics (Belgium)

522 trapping column followed by elution into 50 cm PharmaFluidics analytical column. Separation

523 was achieved through applying a gradient from 5–27% ACN in 0.1% formic acid over 180 min

524 at 200 nl/min. Electrospray ionization was enabled through applying a voltage of 2 kV using a

525 home-made electrode junction at the end of the microcapillary column and sprayed from

526 stainless steel 4 cm needles (PepSep, Denmark). The HFX Orbitrap instrument was operated in

527 data-dependent mode for the mass spectrometry methods. The mass spectrometry survey scan

528 was performed in the Orbitrap in the range of 400 –1,400 m/z at a resolution of 1.2×105,

529 followed by the selection of the twenty most intense ions (TOP10) for HCD-MS2 fragmentation

530 in the Orbitrap using a precursor isolation width window of 0.7 Th, AGC setting of 50,000, and a

531 maximum ion accumulation of 200 ms. Singly charged ion species were not subjected to HCD

532 fragmentation. Normalized collision energy was set to 34 V and an activation time of 1 ms. Ions

533 in a 10 ppm m/z window around ions selected for MS2 were excluded from further selection for

534 fragmentation for 90 seconds. Raw data were submitted for analysis in Proteome Discoverer 2.4.

535 (Thermo-Fisher, CA) software. Assignment of MS/MS spectra were performed using the Sequest

536 HT and Byonic v3.5 (Protein Metrics, CA) algorithms by searching the data against a protein

537 sequence database including all entries from Zebrafish database and other known contaminants

538 such as human keratins and common lab contaminants. Sequest HT and Byonic searches were

539 performed using a 10 ppm precursor ion tolerance and requiring each peptides N-/C termini to

540 adhere with Trypsin protease specificity, while allowing up to two missed cleavages. 6-plex

541 TMT tags on peptide N termini and lysine residues (+229.162932 Da) was set as static

542 modifications while methionine oxidation (+15.99492 Da) was set as variable modification and

543 deamidation of Asparagine and Glutamine amino acids. An MS2 spectra assignment false

544 discovery rate (FDR) of 1% on protein level was achieved by applying the target-decoy database

545 search. Filtering was performed using a Percolator [51] (64bit version).

546 For quantification, a 0.02 m/z window centered on the theoretical m/z value of each the

547 six reporter ions and the intensity of the signal closest to the theoretical m/z value was recorded.

548 Reporter ion intensities were exported in result file of Proteome Discoverer 2.4 search engine as

549 an excel tables. The total signal intensity across all peptides quantified was summed for each

550 TMT channel, and all intensity values were adjusted to account for potentially uneven TMT

551 labeling and/or sample handling variance for each labeled channel. All further data evaluation for

552 statistically differential analysis were performed on in-house made R package based on

553 Bioconductor programs (https://www.bioconductor.org/).

554

555 Immunofluorescence Staining

556 Mouse embryos were harvested at 14.5 days post conception. Fetal livers were dissected and

557 stored in 4% paraformaldehyde at 4°C overnight. Samples were dehydrated in 30% sucrose for 8

558 hours and embedded in OCT. Cryosections were collected at a thickness of 10 microns. Slides

559 were washed three times in PBS + 0.1% Triton, blocked with 5% normal goat serum and 1%

560 bovine serum albumin for two hours, and stained overnight with rabbit anti-c-Kit (Cell Signaling

561 Technology #3074, 1:400) and rat anti-F4/80 (abcam ab6640, 1:100). Slides were washed five

21

562   times with PBS + 0.1% Triton and stained for two hours with Goat anti-rabbit Alexa Fluor 488

563   (Invitrogen A11008, 1:500), Goat anti-rat Alexa Fluor 568 (Invitrogen A11077, 1:500) and

564   DAPI (abcam ab228549, 1:1000). Slides were washed 5 times with PBS + 0.1% Triton and

565   coverslips were mounted with ProLong^{TM} Diamond Antifade Mountant.

566

567   Zebrafish EdU Labeling

568   Embryonic circulation was injected at 72 hpf with 1 nanoliter of 500μM EdU. Embryos were

569   kept at 4°C for 1 hour, fixed in 4% paraformaldehyde for 1 hour, permeabilized with 0.1% Triton

570   for 20 minutes at room temperature and labeled with Alexa Fluor 647 using the Click-iT reaction

571   (Thermo Fisher) for 30 minutes according to manufacturer instructions. Embryos were then

572   washed with PBS+0.5% Triton and blocked for one hour with 10% Normal Goat Serum, 0.5%

573   Bovine Serum Albumin, 0.5% Triton. Samples were incubated with Rat anti-mCherry Alexa

574   Fluor 594 (Invitrogen M11240, 1:200) for one hour at room temperature and washed 5 times

575   with PBS+0.5% Triton.

576

577   Parabiosis

578   Parabiotic zebrafish generated as previously described [52]. Briefly, zebrafish embryos were

579   injected with morpholinos, and incubated until the 1,000-cell stage. Pairs were fused by

580   embedding in 4% methylcellulose, immersion in high-calcium Ringer's solution containing

581   penicillin and streptomycin, and surgical wounding and connection of partner embryos at the

582   animal pole.

583

584   Acridine Orange Staining

585   Acridine Orange dye (Invitrogen A3568) was used at a final concentration of 3μg/mL in E3

586   embryo media. Embryos were incubated with dye for 30 minutes, washed twice with E3, and

587   mounted for imaging.

588

589   Statistical analysis

590   Graphs and statistical analyses were done with Prism (Graphpad), Excel (Microsoft), and

591   RStudio. For all graphs, error bars indicate mean +/- standard deviation. P values were obtained

592   with two-tailed Student's t-¬test or One-way ANOVAs for all analyses as indicated.

593   **Supplementary Materials**

594   Figs. S1 to S5

595   Tables S1 to S2

596   Movies S1 to S3

597

608   **Author contributions:** SJW designed the study, funded the project, performed experiments,

609   managed the project, interpreted the data, and wrote the manuscript. MLS. performed

610 experiments, managed the project, interpreted the data, and edited the manuscript. CPR, EJH,

611 and BB performed experiments and interpreted the data. LIZ designed the study, funded and

612 supervised the project, interpreted the data, and edited the manuscript. All authors reviewed the

613 manuscript.

614 **Competing interests:** LIZ is a founder and stockholder of Fate Therapeutics,

615 CAMP4Therapeutics, and Scholar Rock. All other authors declare that they have no competing

616 interests.

617 **Data and materials availability:** All data are available in the main text or the supplementary

618 materials. The scRNA-seq data have been submitted to the NCBI Gene Expression Omnibus and

619 accession numbers will be forwarded upon receipt. Proteomic data has been submitted to the

620 MassIVE database and PRIDE repository and accession numbers will be available upon receipt.
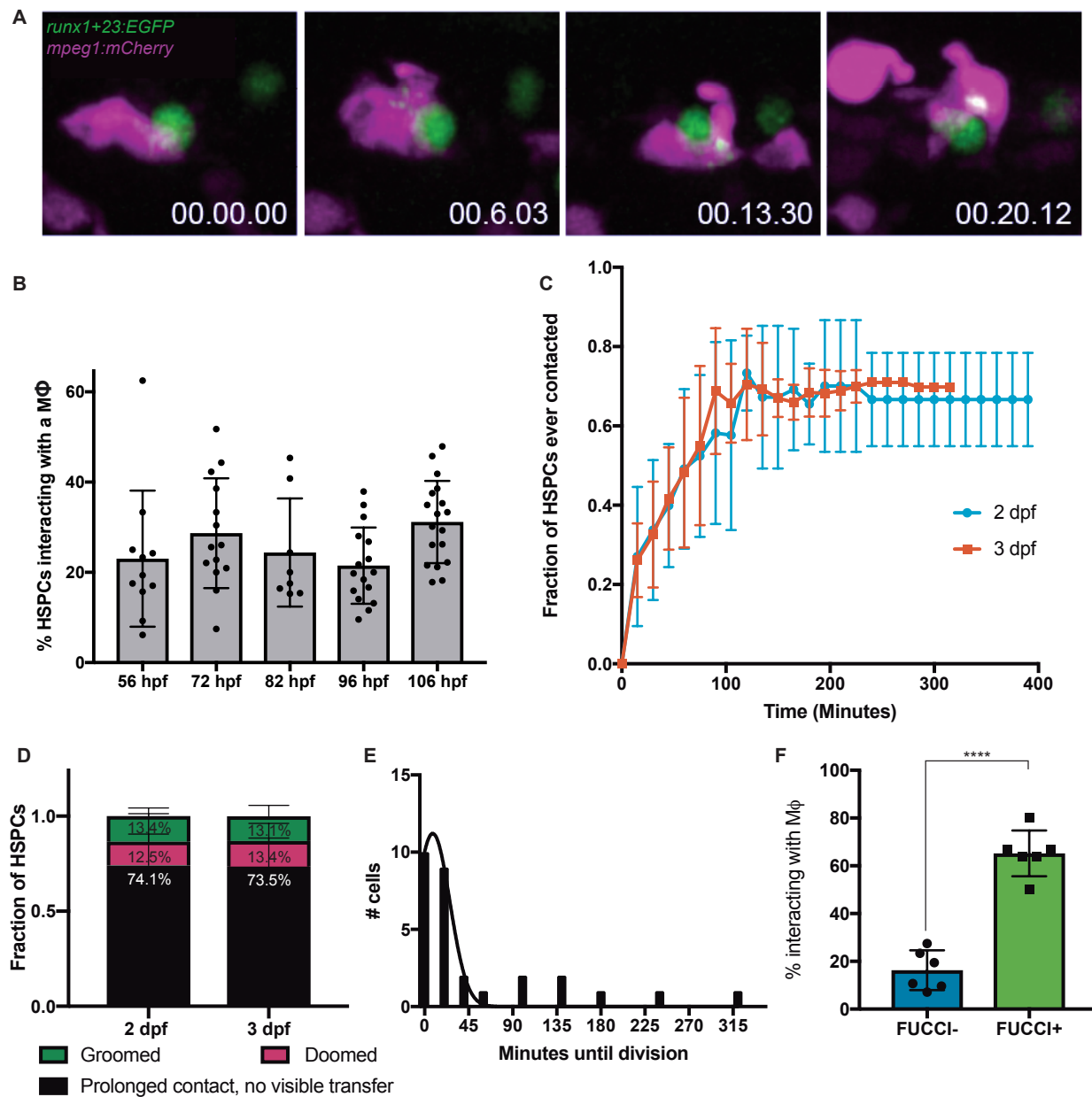
621

622

623

Figure 1

624

625

626   **Fig. 1. Macrophages make intimate interactions with newly formed HSPCs.** (**A**) Time lapse

627   live-imaging identifies prolonged cell-cell contacts between *runx1+23:EGFP$^+$* HSPCs and

628   *mpeg1:mCherry$^+$* primitive macrophages in which cytoplasmic fluorescent material is

629   exchanged. Time is given in hh:mm:ss. (**B**) Approximately 20-30% of HSPCs interact with

630   macrophages in the CHT at any one time from 56 hpf to 106 hpf. Mean +/- s.d. (**C**) High-

631   resolution cell tracking of individual *runx1+23:mCherry$^+$* cells over several hours in the CHT

632   reveals that the majority of HSPCs eventually make sustained contact with macrophages (> 5

633   minutes). Mean +/- s.d. (**D**) Approximately 26% of contacted cells are either groomed or

634   doomed. Mean +/- s.d. (**E**) HSPCs frequently complete a cell division shortly after macrophage

635   interactions. Approximately 81% of HSPCs complete a division within 30 minutes of interacting

636   with a macrophage. Mean +/- s.d. (**F**) Around 65% of Fucci$^+$ HSPCs in G2/M phase interact with

637   macrophages at any one time, as compared to less than 20% of Fucci$^-$ HSPCs. Mean +/- s.d.,

638   Unpaired t test; ****P<0.0001.
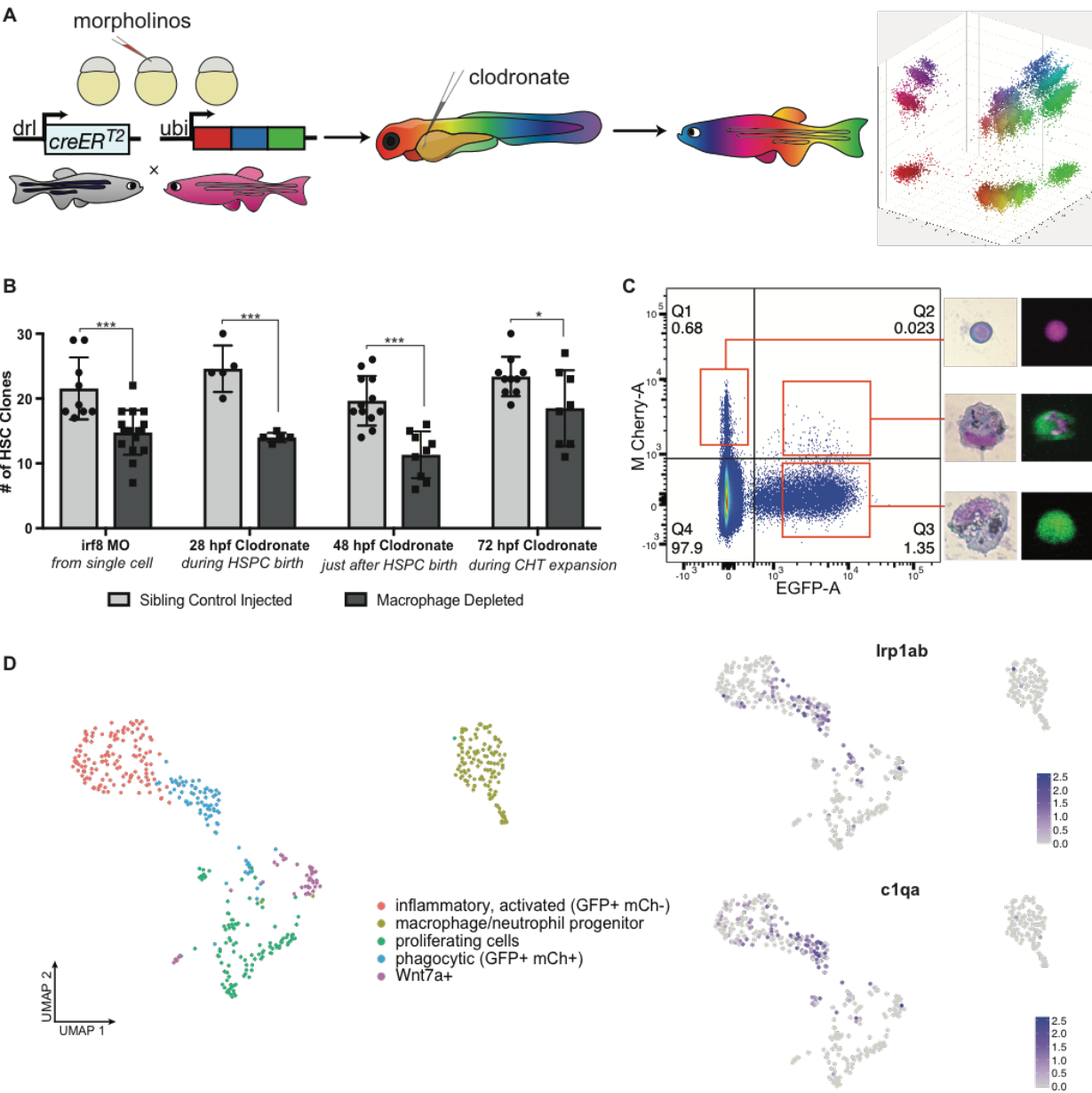
639

Figure 2

642 **Fig. 2. Macrophages in the CHT regulate stem cell clonality.** (**A**) A schematic overview of the

643 *Zebrabow-M* system: animals with 15-20 insertions of tandem multicolor fluorescent cassettes

644 are crossed to a *draculin:CreER^{T2}* line, which enables specific clonal labeling of the lateral plate

645 mesoderm lineage. By treating animals with 4-OHT at 24 hpf just after HSC specification,

646 individual stem cells express unique fluorescent hues. These unique hues can be identified in

647 adult marrow and quantified to determine the number and size of stem cell clones. (**B**) Families

648 of *Zebrabow-M;draculin:CreER^{T2}* animals injected with either clodronate liposomes or the *irf8*

649 morpholino exhibit reduced numbers of HSC clones in the adult marrow, even when

650 macrophages are not depleted until after emergence from the VDA. Mean +/- s.d., Unpaired t

651 test; *P<0.05, ***P<0.001. (**C**) Macrophages (*mpeg1:EGFP^+*) which have interacted with

652 HSPCs (*runx1+23:mCherry^+*) and removed fluorescent material can be identified and harvested

653 by flow cytometry. (**D**) Uniform Manifold Approximation and Projection (UMAP) plots shows

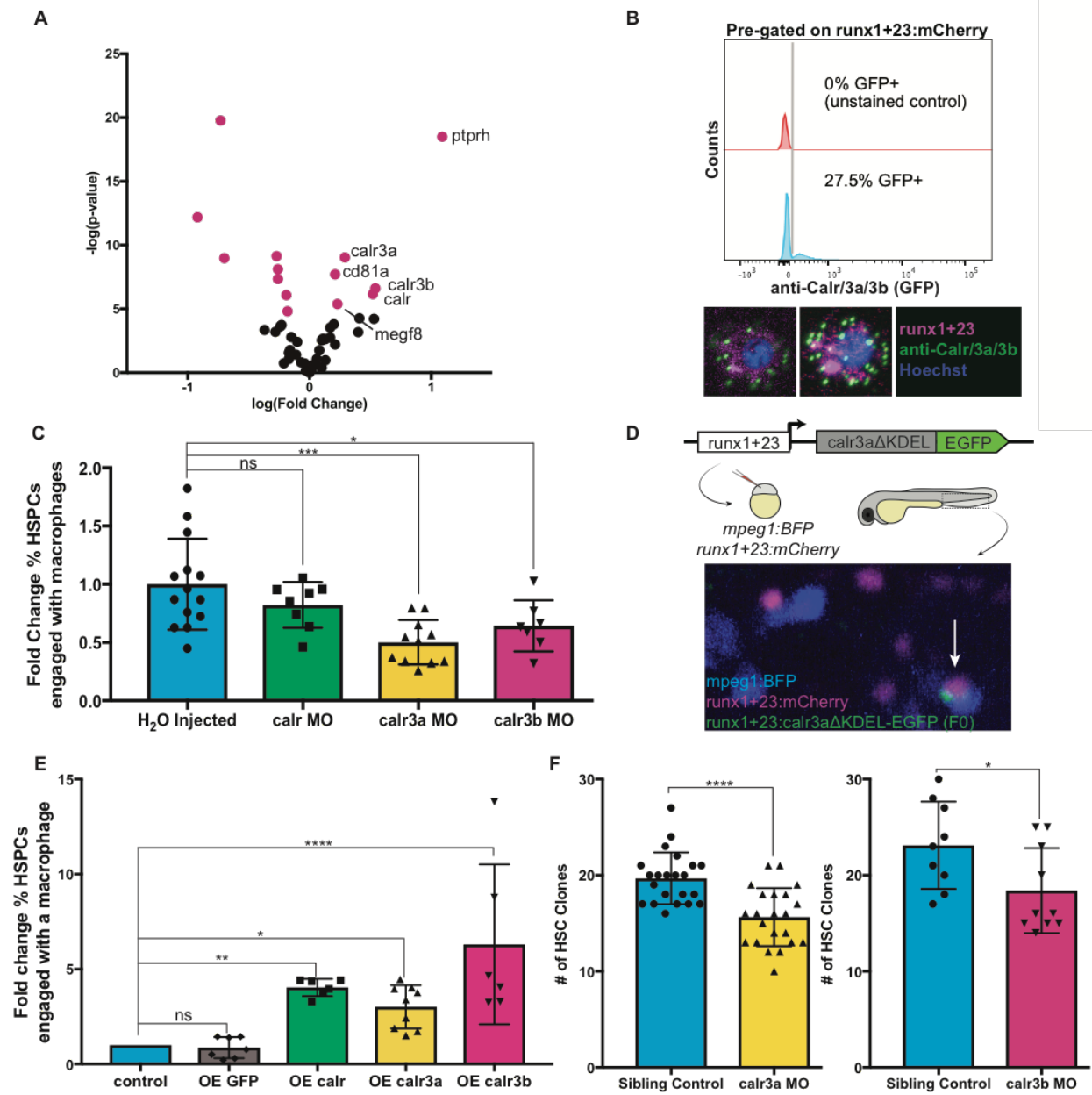654 that macrophages which engage HSPCs are marked by *lrp1ab* and *c1qa*. Spectral scale reports z-

655 scores.

656

Figure 3

657

658

659   **Fig. 3. Calreticulin drives HSPC-macrophage interactions to regulate clonality.**

660   (**A**) Hundreds of interacting and noninteracting macrophages were sorted and processed for few-

661   cell proteomics by LC-MS/MS. Analysis of differentially enriched putative surface proteins from

662   interacting macrophages identifies three paralogs of Calreticulin. Magenta dots indicate

663   differentially enriched surface proteins. (**B**) Antibody staining and flow cytometry identifies

664   ~30% of live *runx1+23:mCherry*$^+$ HSPCs stain positive for Calreticulin. Confocal imaging

665   displays punctate surface stain, similar to previous reports. (**C**) Knock-down of *calr3a* or *calr3b*

666   by morpholino injection significantly reduces the fraction of HSPCs interacting with

667   macrophages at any one time. Data are normalized to H_2O injected embryos. Mean +/- s.d., One-

668   way ANOVA with Dunnett's multiple comparisons test; *$P<0.05$, ***$P<0.001$. (**D**) Schematic

669   and example of overexpression approach. Calreticulin paralogs lacking the ER-retention KDEL

670   sequence were fused to EGFP, driven by the HSPC-specific *runx1+23* enhancer, and injected

671   into stable *runx1+23:mCherry;mpeg1:BFP* embryos to generate mosaic animals to compare

672   HSPCs overexpressing Calreticulin against unperturbed HSPCs in the same embryo. Arrow

673   indicates an HSPC overexpressing *calr3a* engaged by a macrophage. (**E**) HSPCs overexpressing

674   *calr, calr3a*, or *calr3b* are more frequently engaged by macrophages compared to non-

675   overexpressing HSPCs in the same embryos. Overexpressing GFP alone has no effect on

676   macrophage engagement. Data are normalized to the fraction of non-overexpressing HSPCs in

677   each individual animal. Mean +/- s.d., One-way ANOVA with Dunnett's multiple comparisons

678   test; *$P<0.05$, **$P<0.01$, ****$P<0.0001$. (**F**) Inhibition of *calr3a* or *calr3b* by morpholino

679   injection reduces the number of HSC clones that contribute to adult marrow compared to control

680   injected embryos from the same family. Mean +/- s.d., Unpaired t test; *$P<0.05$, ****$P<0.0001$.
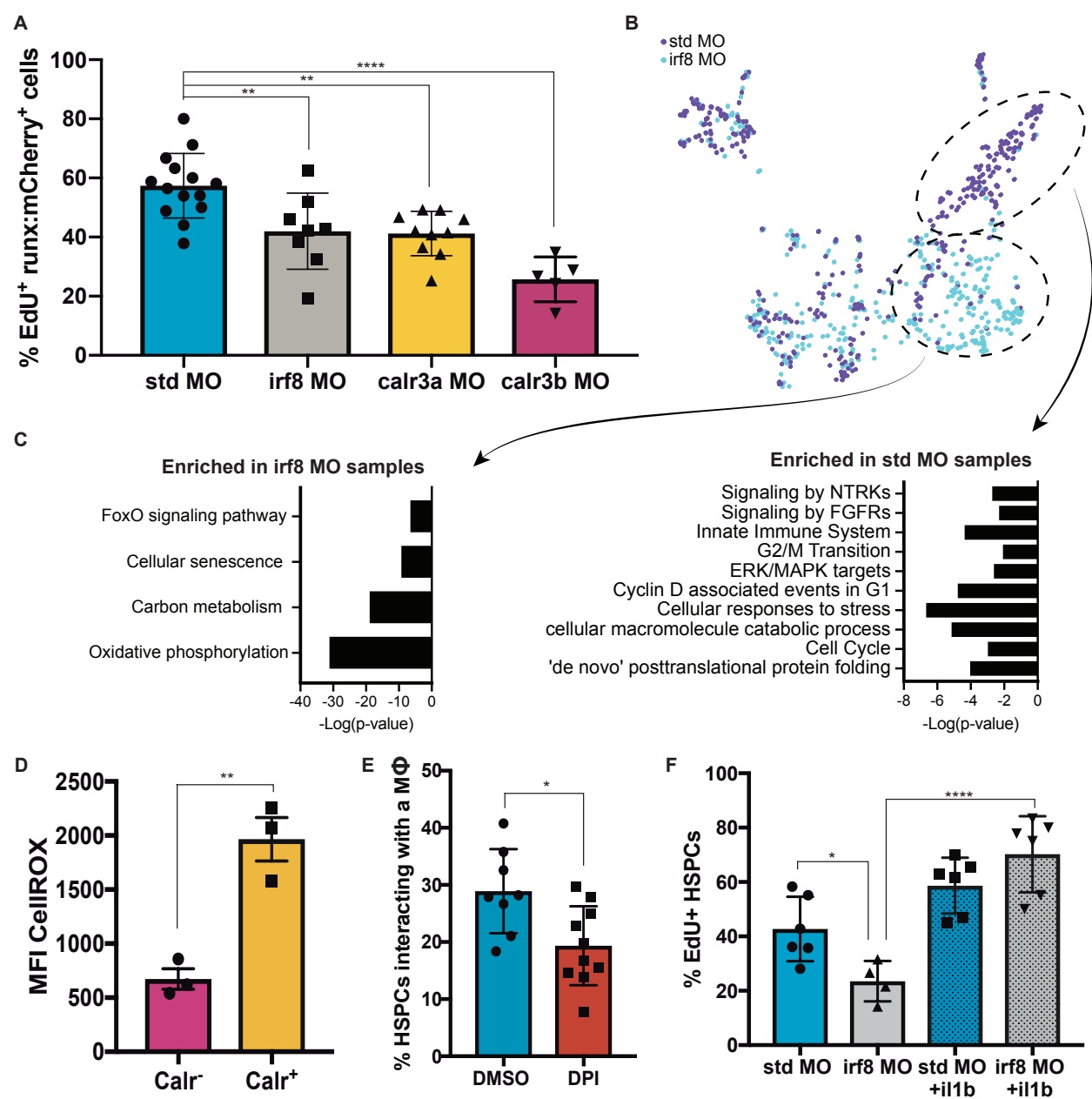
681

Figure 4

684   **Fig. 4. Macrophages buffer HSPC stress and regulate HSPC expansion.**

685   (**A**) EdU staining of *runx1+23:mCherry* embryos injected with either the *calr3a*, *calr3b*, or *irf8*

686   morpholinos identifies a significant reduction in the fraction of proliferating HSPCs in the CHT

687   at 3 dpf. Mean +/- s.d., One-way ANOVA with Dunnett's multiple comparisons test; **P<0.01,

688   ****P<0.0001. (**B**)(**C**) Single-cell mRNA-seq analysis of *runx1+23*$^+$ FACS purified cells from 3

689   dpf embryos injected with either the *irf8* or non-targeting control morpholino. Subsets of HSPCs

690   are enriched in the *irf8* or control sample. KEGG enrichment pathways reveals a population of

691   stressed HSPCs that persist in the absence of macrophages and a population of cycling cells

692   enriched in the control sample. (**D**) Embryonic HSPCs marked by surface Calreticulin exhibit

693   higher levels of ROS as marked by CellROX intensity. (**E**) Inhibition of ROS by drug treatment

694   with the NADPH oxidase inhibitor, diphenylene iodonium (DPI), significantly reduces the

695   fraction of HSPCs engaged by macrophages in the CHT. Mean +/- s.d., Unpaired t test; *P<0.05.

696   (**F**) Expression of *il1b* by heat shock is able to rescue the effect of macrophage depletion on

697   HSPC proliferation. Mean +/- s.d., One-way ANOVA with Sidak's multiple comparisons test;

698   *P<0.05, ****P<0.001.

699